

Beyond Weber's Law: A Second Look at Ranking Visualizations of Correlation

Roy G. Biv, Ed Grimley, Member, IEEE, and Martha Stewart

Abstract—Models of human perception — including perceptual “laws” — can be valuable tools for deriving visualization design recommendations. However, it is important to assess the explanatory power of such models when using them to inform design. We present a secondary analysis of data previously used to rank the effectiveness of bivariate visualizations for assessing correlation (measured with Pearson’s r) according to the well-known Weber-Fechner Law. Beginning with the model of Harrison *et al.* [1], we present a sequence of refinements including incorporation of individual differences, log transformation, censored regression, and adoption of Bayesian statistics. Our model incorporates all observations dropped from the original analysis, including data near ceilings caused by the data collection process and entire visualizations dropped due to large numbers of observations worse than chance. This model deviates from Weber’s Law, but provides improved predictive accuracy and generalization. Using Bayesian credibility intervals, we derive a partial ranking that groups visualizations with similar performance, and we give precise estimates of the difference in performance between these groups. We conclude with a discussion of the value of data sharing and replication, and share implications for modeling similar experimental data.

Index Terms—TBD

INTRODUCTION

Perceptual laws, such as Weber’s Law, offer the tantalizing potential to explain differences in the performance of visualizations, simplify design recommendations, and drive automated visualization systems. However, many such laws have long been studied — not without controversy [cite] — using simple models that aggregate individual differences before modelling. Harrison *et al.* [1] follows from this tradition, investigating the relationship between the correlation of two variables (measured using Pearson’s r) and the precision of people’s estimates of that correlation using different visualizations (measured using just-noticeable differences). In accordance with Weber’s Law, they fit linear regressions to the means of the just-noticeable differences for each value of r in each condition, not to the individual observations directly.

By removing a large portion of the variance in the data (individual differences), they could not use their parametric model to make predictive inferences. Instead, they employed non-parametric tests to examine differences between visualization types, which complicates the estimation of effect sizes. Even if we establish that one visualization is better than another, we would like to know by how much in order to judge whether the difference is meaningful in practice. Ideally we would like to know this effect size on some interpretable scale (such as in terms of just-noticeable differences in r), which is made difficult when using non-parametric tests.

In this paper, we conduct a secondary analysis of the data in Harrison *et al.* [1]. Much of this paper focusses on understanding and accounting for individuals’ differences in precision of estimation in order to derive parametric models that can predict the expected precision of each visualization technique. Given an appropriate parametric model, we can estimate interpretable differences between visualization types (e.g., as a ratio of just-noticeable differences) in order to judge whether these differences have practical significance.

We begin by revisiting the experimental setup and subsequent data analysis of Harrison *et al.* [1]. We then progress through a series of model refinements, starting with a basic linear model. We first address problems of non-constant variance, presenting evidence that a log-linear model — which does not follow Weber’s Law — better describes the relationship between just-noticeable differences and objective correlation. We then augment our model with censored regression to include all observations in the analysis, including outliers, data near ceilings and floors resulting from features of the data collection process, and entire visualizations originally dropped due to large numbers of data points worse than chance.

This model allows us to directly and quantitatively answer questions left largely unaddressed by the original paper: given a dataset with unknown correlation, how well would we expect each visualization technique to perform (and what is the uncertainty associated with this estimate)? What are the expected differences in performance? Which visualizations are effectively equivalent? We identify clusters of visualizations with similar precision and quantify the expected difference in precision between clusters, yielding a comprehensive set of practical recommendations in the form of a partial ranking of visualizations of correlation. This partial ranking provides concrete guidance to practitioners by grouping visualizations with similar performance and by giving precise estimates of the difference in performance between groups of visualizations.

Finally, we discuss the applicability of similar models to other problems of estimating the perceptual performance of visualizations from experimental data. Censored regression offers a flexible way to account for a class of experimental artifacts likely to be found in other perceptual experiments in visualization, and examination of individual differences in general yields models with greater explanatory power.

1 BACKGROUND

- Roy G. Biv is with Starbucks Research. E-mail: royg.biv@aol.com.
- Ed Grimley is with Grimley Widgets, Inc.. E-mail: ed.grimley@aol.com.
- Martha Stewart is with Martha Stewart Enterprises at Microsoft Research. E-mail: Martha.stewart@marthastewart.com.
- Manuscript received 31 Mar. 2014; accepted 1 Aug. 2014; date of publication xx xxx 2014; date of current version xx xxx 2014.

For information on obtaining reprints of this article, please send e-mail to: tvcg@computer.org.

Might be some useful pieces about perceptual laws to put in here. The controversy around them might be most useful, etc. Known limitations of that approach (e.g. stuff about power laws for judging area?)

- Jeff: Good things to note are that in addition to Weber's Law studies, the classic Steven's work also averages individual responses. Some folks have proposed "auto-correcting" area visualizations by scaling the areas in accordance with a Steven's law exponent to get perceptual linearity. However,

1. To fit a Weber model as in Harrison et al., we **take the mean** in each $r \times$ approach (**from below** or **from above**).

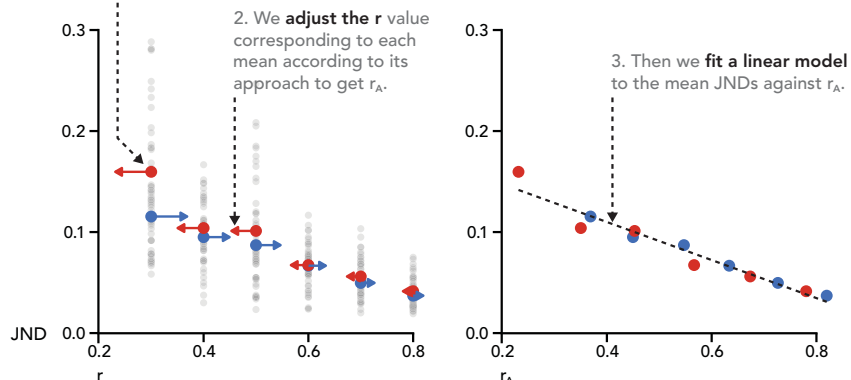


Fig. 1. High-level comparison of the Weber's Law-based modelling approach of Harrison et al. [1] and the approach taken in this paper as applied to the scatterplot-positive condition.

Cleveland has a nice short experiment showing why individual differences undermine this approach: W. S. Cleveland, C. S. Harris, and R. McGill. Judgements of Circle Sizes on Statistical Maps. *Journal of the American Statistical Association*, 77:541–547, 1982.

1.1 Harrison et al. experimental setup

- Should briefly describe original paper's experimental setup
- Need to define the variables in the experiment: visualization, direction, approach, r , JND
- # participants, etc etc

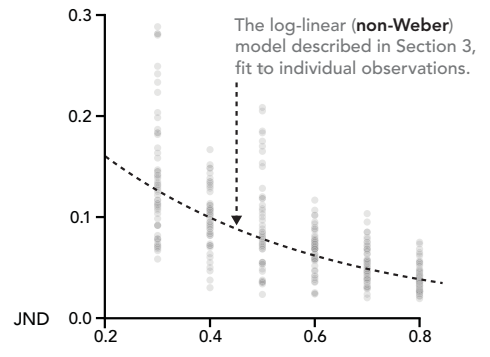
1.2 Harrison et al. analysis

Harrison et al. [1] used an analysis approach common in prior work on Weber's law, such as Rensink & Baldridge [2] (also Stevens' Power Law). First, they took the mean of all individual observations of JND within each condition (where each condition is defined as a unique combination of visualization \times direction \times approach $\times r$). They then modelled the relationship between the value of r and that within-condition mean JND. Thus, their model describes the relationship between the mean performance of a group of people from the population, but not the performance of any individual.

What this omits is any sense of the variance in individual performance, which diminishes the explanatory power of such models. For example, it may be that visualization A exhibits high precision of estimation (low JND) in the average case — but that its variance is higher than visualization B , which performs slightly worse on average but which is more consistent across individuals. Without considering variance, we have no way of knowing whether such differences exist, and we may be led (for example) to choose to deploy a visualization that has slightly better average-case performance but which elicits much worse performance for some substantial portion of the population. This is exactly the problem of the *bias-variance tradeoff*, well-known in machine learning [3]. From a design perspective, this is not unlike an architect who designs every home for the average family of 2.6 people. Individuals, not group means, digest visualizations.

Such an analysis also obscures problems with model fit by discarding large portions of the variance (essentially all individual variation) and reducing a large sample of data to comparatively few data points. This explains why Harrison et al. [1] (like Rensink & Baldridge [2]) found very high R^2 values describing the fit of their models (as high as 0.98 for one visualization). But when we attempt to interpret these values of R^2 — for example, as the percent of variation explained by the model — something is missing. 98% of individual variation is not explained by this model, as individual variation was discarded before the model was fit. We might instead interpret this as indicating 98%

In this paper, we instead aim to **fit models to individual observations** in order to understand individual (not just group mean) performance.



of the variation in the location of the mean was explained, but this is a much less useful thing to know if we wish to understand how *individuals* perceive visualizations. As we will see below, if we try to fit linear models to individual observations directly, the linear model does not exhibit the best fit.

Finally, because of the poor fit of the linear model to individual observations, we cannot use the fitting error to estimate significant differences between conditions. Indeed, despite being a paper that proposes a parametric model to describe the performance of each visualization, Harrison et al. do not use their parametric models to estimate differences between conditions; they use the nonparametric Wilcoxon rank-sum test. In this paper we propose a model of sufficient specificity that parametric estimation of differences becomes straightforward; this allows us to not only examine the differences between conditions but to clearly describe the expected magnitude of those differences (i.e., effect sizes) using parameters from the model. By employing parametric models, we have the advantage of interpretable effect sizes — for example, ratios of just-noticeable differences, from which we can say, “*visualization A* is x times more precise than *visualization B*” — that are not easily gleaned from nonparametric tests.

2 MODEL 1: LINEAR MODEL

We begin our secondary analysis by incorporating individual differences to model just-noticeable differences directly on raw values of r . A first pass at this would be to simply use a linear regression. Such a model might look like:

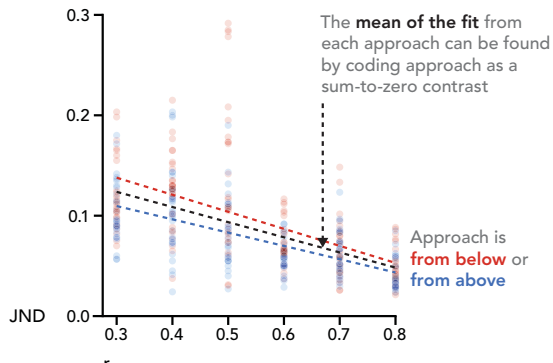
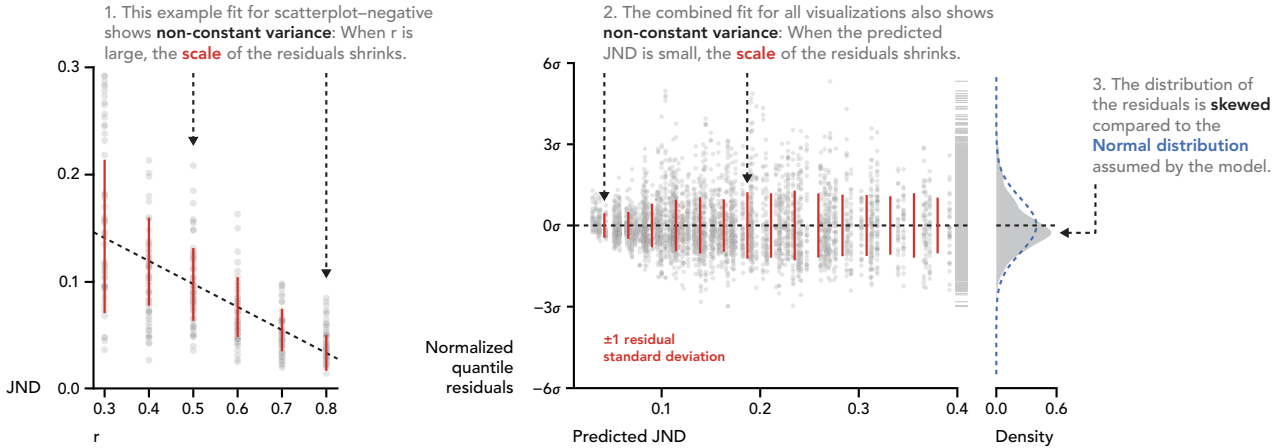


Fig. 2. Example of data and linear regression fits for the different values of approach for parallel coordinates-negative.

$$y_{i,v} = \beta_{v,1} + \beta_{v,2}r_i + \epsilon_i$$

$$\epsilon_i \sim \mathcal{N}(0, \sigma_v^2)$$

A. LINEAR MODEL



B. LOG-LINEAR MODEL

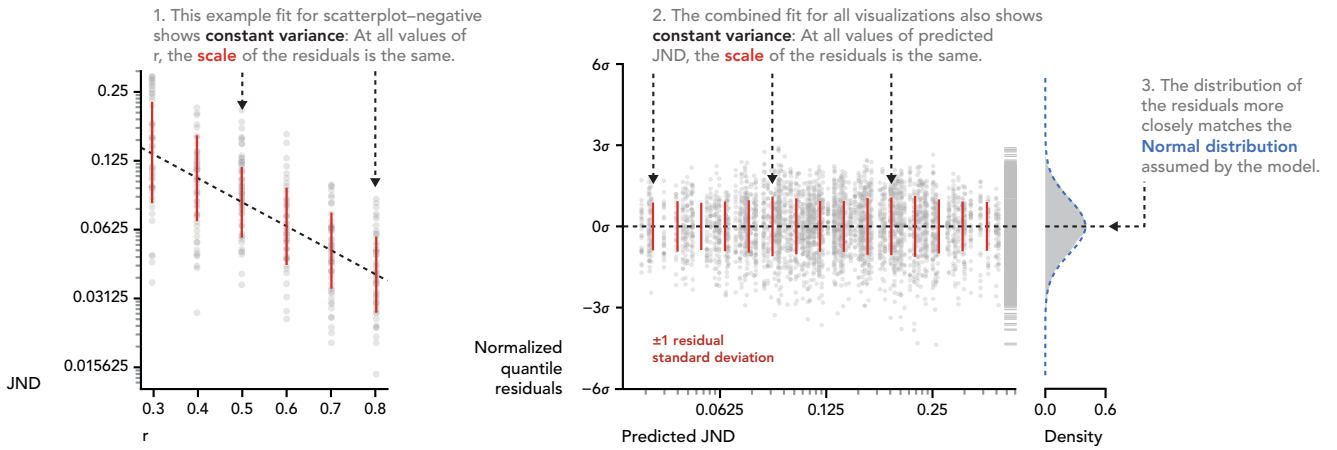


Fig. 3 Comparison of fits of the linear model (Section 2) and the log-linear model (Section 3). Example fits of each model to scatterplot-negative are shown in A.1 and B.1. Plots of normalized residuals for all visualization \times direction pairs are shown in A.2 and B.2. Density plots of normalized residuals with comparison to the standard normal distribution are shown in A.3 and B.3.

This is a fairly standard linear regression. Here we say that, for each visualization \times direction pair v , each JND ($y_{i,v}$) is equal to a linear function of r_i with intercept $\beta_{v,1}$ and slope $\beta_{v,2}$ plus some normally-distributed error ϵ_i . Note that the intercept, slope, and variance of the error (σ_v) are all dependent on v , the particular visualization \times direction pair.

Unfortunately, this straightforward model leaves out consideration of *approach* — half of the JNDs were determined by a procedure having people compare the reference r to higher values of r (*an approach from above*), and half compared to lower values of r (*from below*). When the approach is from above, the values of JND are underestimated (because higher values of r tend to have lower JND), and when the approach is from below, JND is overestimated. This effect is visible in Fig. 2: note the two systematically different estimates of JND depending on approach. Harrison *et al.* used the correction described by Rensink & Baldridge [2] to address this: they adjusted the value of r by moving it up by half the mean JND at that value of r when from above, and down by half the mean JND when from below.

However, this adjustment is only well-defined if we are using the within-condition means of r as our unit of analysis. When fitting a model to individual observations, we must find another way to account for approach. Again consider Fig. 2: because each condition causes a bias in the opposite direction, we could take the average of the two fit lines to approximate the outcome y for each r (the black line in Fig. 2). Such a model can be fit by including *approach* and its interaction

with r in the regression. We code *approach* as a sum-to-zero contrast, defined by the variable a_i :

$$a_i = \begin{cases} -1, & \text{if } \textit{approach} \text{ is } \textit{from above} \\ 1, & \text{if } \textit{approach} \text{ is } \textit{from below} \end{cases}$$

We then add the effects of *approach* and *approach* \times r to the model (new terms in red):

$$\begin{aligned} y_{i,v} &= \beta_{v,1} + \beta_{v,2}r_i + \beta_{v,3}a_i + \beta_{v,4}a_ir_i + \epsilon_i \\ \epsilon_i &\sim \mathcal{N}(0, \sigma_v^2) \end{aligned}$$

Because these are sum-to-zero contrasts, the overall slope ($\beta_{v,1}$) and intercept ($\beta_{v,2}$) for r are defined with respect to the mean of the two levels of a_i — in other words, the slope and intercept describe the mean of the slope and intercept of the *above* and *below* levels, exactly the black line in Fig. 2.

2.1 Problems with the linear model

The linear model¹ exhibits several issues of fit that indicate violations of model assumptions, illustrated in Fig. 3A. Two such issues in particular are *non-constant variance* and *skewed residuals*, both of which are violations of the assumptions inherent in the distribution of the error term ϵ_i .

Non-constant variance (heteroscedasticity). As defined in the model, the variance of the error, σ_v^2 , is constant with respect to r . That is, for a given visualization \times direction pair v , the variance of y (the JND) is assumed to be the same no matter what the value of r is. Fig. 3A.1 shows a sample plot of the model fit for scatterplot-negative: we can see that when r is high, the variance of the residuals gets smaller, violating this assumption.

We can assess this assumption for all visualization \times direction pairs simultaneously by examining the differences between the observed JNDs and their predicted values (the *residuals*). If the constant variance assumption holds, the scale of the residuals should be the same for all predicted values of JND. Fig. 3A.2 shows that at low values of JND, the variance of the residuals is lower than at higher values of JND. This is consistent with the example fit of scatterplot-negative, as low values of JND correspond to high values of r . Non-constant variance is common in data with a well-defined lower bound: here, JND cannot be less than 0, and as we approach 0, performance tends to cluster together more tightly.

Skewed residuals. Data with a lower bound also often exhibits the second model violation seen here: skewed residuals (more generally, non-normal residuals). We can think of JND as “bunching up” the closer it gets to 0; besides resulting in less variance, this also explains the skew in the residuals seen in Fig. 3A.3. The residuals do not follow a normal distribution, which is not unexpected given the bounded nature of the data. While it is sometimes the case that we can get away with assuming bounded data is normally-distributed, such simplifications tend to break down the closer we get to the boundaries; here, the assumptions are clearly violated and suggest we should consider other models. This makes sense: looking at Fig. 3A.1, JND gets quite close to the 0 boundary.

3 MODEL 2: LOG-LINEAR MODEL

Fortunately, a log transformation of the response is often sufficient in cases of non-constant variance and skewed residuals to solve both problems simultaneously, and often shows up in models of human performance. The applicability of such a transformation is hinted at here as the residual distribution has the approximate appearance of a log-normal distribution.² This transformation also has the useful property that the resulting model retains some interpretability: coefficients of this model that describe additive differences on the log-scale correspond to multiplicative differences on the original data scale (in other words, we will be able to use this model to make claims like, “*visualization A* yields x times the precision of *visualization B* for estimating correlation”). The log-linear model, which deviates from Weber’s Law, is as follows:

$$\begin{aligned}\log(y_{i,v}) &= \beta_{v,1} + \beta_{v,2}r_i + \beta_{v,3}a_i + \beta_{v,4}a_ir_i + \epsilon_i \\ \epsilon_i &\sim \mathcal{N}(0, \sigma_v^2)\end{aligned}$$

Comparing the residual fit of the log-linear model to the linear model (Fig. 3B), we can see that the fit no longer suffers from problems of non-constant variance or skewed residuals. This fit also exhibits lower AIC than the linear model (-11683 versus -10037), indicating greater

predictive validity.³ The residual distribution more closely matches the normal distribution assumed by the model. In addition, because all values in $(-\infty, +\infty)$ are mapped onto $(0, +\infty)$ by the log transformation, we have solved another problem for free: the linear model can make nonsensical predictions, such as JNDs that are less than 0, that the log-linear model does not.

3.1 Data dropped from the analysis so far

So far, we have restricted our analyses to those data points analysed in the original work. The original work used two criteria to exclude data from analysis:

Outliers. Within each condition (visualization \times direction \times approach $\times r$), observations outside of 3 median absolute deviations from the median were dropped from the analysis. The original paper justified this as a way to address non-normality in the data (although as we have seen above, it did not). Since we have addressed the issue of normality through log transformation, this criteria is no longer particularly relevant. Since our goal is to explain as much of the data as possible, we believe there is no additional need to drop outliers from the analysis.

Data worse than chance. In the original work, visualization \times direction pairs with more than 20% of JNDs greater than 0.45 were dropped (6 out of 18 pairs). The 0.45 threshold represents the *chance* threshold for this experiment: values of JND near or beyond this threshold indicate a failure on a participant’s part to judge degree of correlation better than could be done by answering at random. However, removing visualizations with large numbers of observations worse than chance addresses only part of the problem. As can be seen in Figure X, many of the remaining tested visualization \times direction pairs still have observations at or beyond the chance boundary. The problem is that we have excluded certain visualization \times direction pairs for having too many observations worse than chance, but have done nothing to address those observations worse than chance that remain in the visualizations we *do* analyse.

Importantly, in the case of points near or beyond this boundary, we can say that these observations probably represent JNDs of 0.45 or worse, but that we do not know the exact JND due to the constraints of the experiment. This type of data can be analysed using censored regression.

4 MODEL 3: CENSORED LOG-LINEAR MODEL

Censored regression can be used when some of the observed data points do not have a known value, but instead are known to lie above (or below) a certain threshold [4], [5]. While we do not know the exact value of points beyond the threshold, we still know how many points were observed beyond the threshold, and it is this information that we can use to fit the model (see example in Fig. 4). While we cannot reliably observe certain values of JND — either because the setup of the experiment makes them indistinguishable from chance, or because of ceilings and floors in observable JND due to the bounds on r — we can use observations close to or beyond those thresholds to estimate the proportion of values we might expect to see above them.

- Ceiling in JND (when approach is from above) and floor in JND (when from below) also candidates for censoring.
- Derive thresholds

¹ This and all other non-Bayesian models in this paper were fit using the `gamlss` procedure in R [9].

² We can more systematically justify this transformation by fitting a Box-Cox transformation [10] to the data, whose parameter λ describes a power transformation of JND. The Box-Cox procedure for this data estimates $\lambda = 0.0292$ with a 95% confidence interval of [-0.005,

0.0635], which includes 0 (the log transform) and excludes 1 (identity; i.e. the linear model) at $p < 0.00001$ ($\text{LR } \chi^2(1) = 2756.77$).

³ Model comparison by AIC is asymptotically equivalent to leave-one-out cross validation [11]. The log-linear model was fit using a log-normal error distribution (rather than the equivalent log transformation of responses with a normal error distribution shown here) so that its AIC can be compared to the linear model.

- Include example of censored distribution as explanation?
 - o Show example of downward bias at low r in a viz near the chance threshold to demonstrate value of censored models

To incorporate censoring into our model, we first define a censoring threshold, $c_{i,v}$. This threshold varies depending on r and the approach, (see Figure X):

$$c_{i,v} = \begin{cases} \min(0.95 - r_i, 0.4), & a_i = -1 \\ \min(r_i - 0.05, 0.4), & a_i = 1 \end{cases}$$

We use the log-linear model to predict a latent variable y^* instead of y :

$$\log(y_{i,v}^*) = \beta_{v,1} + \beta_{v,2}r_i + \beta_{v,3}a_i + \beta_{v,4}a_ir_i + \epsilon_i$$

$$\epsilon_i \sim \mathcal{N}(0, \sigma_v^2)$$

We redefine y as being equal to the censoring threshold at the corresponding value of r if its observed value is greater than that threshold.⁴ The model then predicts y based on the latent variable y^* and the censoring threshold c :

$$y_{i,v} = \begin{cases} y_{i,v}^*, & y_{i,v}^* \leq c_{i,v} \\ c_{i,v}, & y_{i,v}^* > c_{i,v} \end{cases}$$

4.1 Bias in uncensored model

The censored model allows us to address problems of bias caused by JND being underestimated near the ceilings described above. See Figure X, which compares the censored and uncensored models for visualization XXX. Note that where large amounts of observations are worse than chance, the uncensored model estimates people as having *higher* precision (lower JND) than we should expect! This bias conspires to make a low-performing visualization seem better than it is, motivating our use of censored regression here. This underscores the problem with excluding some visualization \times direction pairs based on the chance criteria without accounting for chance in the pairs we do analyse.

5 MODEL 4: BAYESIAN CENSORED LOG-LINEAR MODEL

In this section we describe a Bayesian variant of the censored log-linear model. In Bayesian modelling, we specify our *prior beliefs* about a model in the form of probability distributions, and then *update* our beliefs based on observed evidence (the data collected in an experiment). These updated beliefs are called *posterior distributions*.

This approach yields a richer estimation of the parameters of interest — complete posterior probability distributions of all parameters — instead of point estimates and confidence intervals. Such posteriors offer an easy way for others to build on our work by using our posterior estimates to inform prior distributions in future work. As we will see, Bayesian estimation also provides a straightforward way to derive the expected performance (with uncertainty) on any hypothetical dataset of correlations that can be expressed as a probability distribution over r . We largely adopt Kruschke's [6] approach to Bayesian experimental statistics by using 95% credibility intervals⁵ of posterior distributions to estimate differences between parameters.

⁴ As a result of this transformation of the responses and the inclusion of data not included in previous models, the censored model cannot be compared to the previous models using AIC. However, we believe the theoretical justification based on ceilings caused by the structure of the experiment and the ability of these models to accommodate data dropped previously motivate the use of censored regression here, and for visualization \times direction pairs far from those ceilings the fit is similar to the non-censored log-linear model.

Consider 5000 samples drawn from a standard normal distribution: the *sample mean* is ~ 0 .

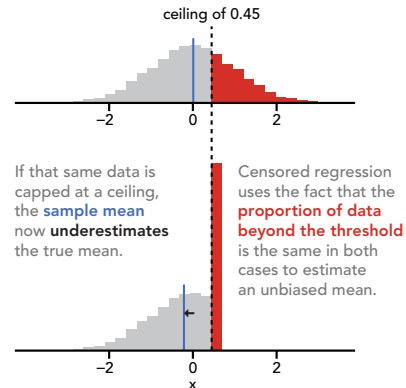


Fig. 4. An example of the use of censored regression to estimate a model when some of the data has been capped at a ceiling.

5.1 Participant effects

As a final refinement to the model, we also incorporate linear mixed effects modelling [1]. Specifically, we add a varying-intercept *random effect* dependent on participant.⁶ This effect helps account for the fact that we have taken multiple measurements from each participant in the experiment (4 each) by modelling each participant's average performance as an offset from the fit line. Without accounting for this, we effectively are treating our data as having 4 times the number of independent observations as we actually have, causing us to overestimate the precision of our parameters (a problem known as *pseudoreplication* [7], which motivates related modelling approaches for repeated measures, such as within-subjects ANOVAs). By incorporating random effects, we improve the generalizability of our estimates of other parameters through accounting for the correlation between observations from the same participant.

We include a random intercept by estimating an offset U_k from the intercept for each participant k :

$$\log(y_{i,v}^*) = \beta_{v,1} + \beta_{v,2}r_i + \beta_{v,3}a_i + \beta_{v,4}a_ir_i + \epsilon_i + U_k$$

$$\epsilon_i \sim \mathcal{N}(0, \sigma_v^2)$$

$$U_k \sim \mathcal{N}(0, \tau_v^2)$$

U_k is called a random effect because each value of it is assumed to be randomly drawn from the distribution $\mathcal{N}(0, \tau_v^2)$. That is, each participant comes from some broader population, and their differences in average performance are distributed normally (on the log scale). The parameter τ_v^2 is the variance of participants' average performance for visualization \times direction pair v . This allows us to estimate how variable participants' performance is within each visualization \times direction pair, which tells us how similar different individuals' estimations are to each other for each visualization. As noted earlier, understanding how individuals vary compared to the rest of the group is an important consideration when deriving design recommendations meant to be applied broadly.

⁵ Though we use 95% quantile intervals instead of 95% highest-density intervals since these are invariant under the log transform.

⁶ Several models with varying slopes and intercepts failed to converge within 1,000,000 iterations, likely due to the small number of observations per participant and the use of censoring. Visual inspection of per-participant slopes suggested low variance in slope, and since our question of interest here is that of variance in average performance more than sensitivity to r , we believe a varying-intercepts model suffices.

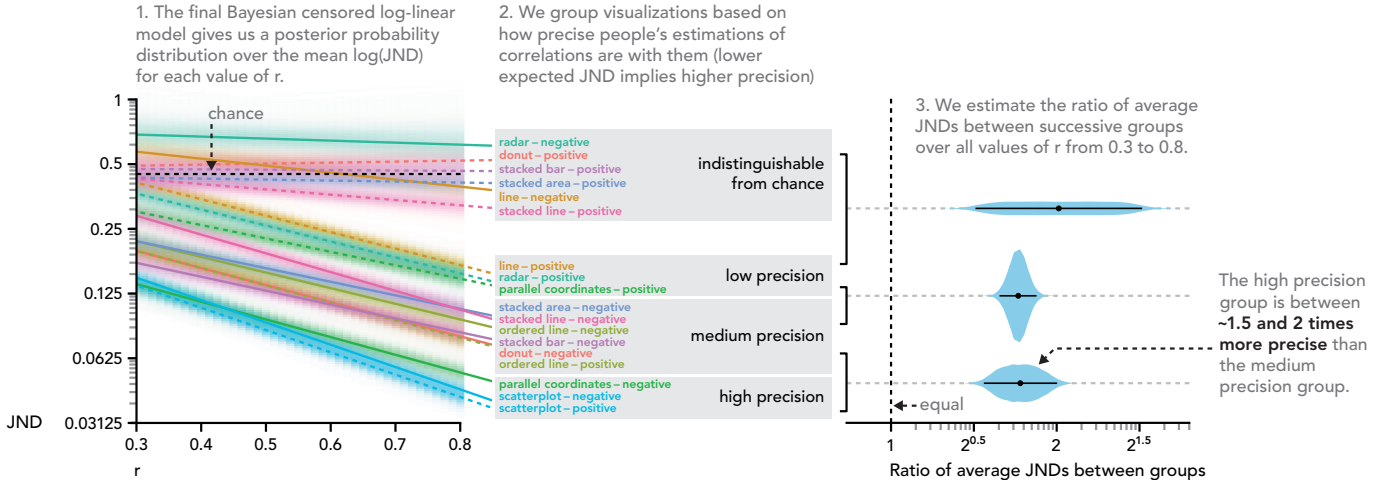


Fig. 6. Final model and partial ranking of visualizations. Part 1 may be compared to Figure 6 from Harrison *et al.*, with several notable differences: our results are on a log scale (suggesting a different fit shape), our results provide uncertainty (even if standard errors had been given in Harrison *et al.* they would not have been valid due to the mean-fitting procedure), and we include all tested visualizations in the analysis. Part 2 may be compared to Figure 7 from Harrison *et al.*, except we provide only a partial ranking (instead of a complete ranking) consistent with the available evidence. Part 3 has no direct analog in Harrison *et al.*. Posterior densities in Part 3 are augmented with median and 95% quantile credibility intervals.

5.2 Priors

In order to fit a Bayesian model, we must also provide *prior distributions* for all unknown parameters. These represent our belief in the location of each parameter prior to running the experiment. In this paper we use weakly-informed priors derived from the results of Rensink & Baldridge [2]. We use weakly-informed priors because we do not have data on all plot types, but can use knowledge of performance on scatterplots to infer what range of performance we should expect on other plot types. The high-level goal of our priors is to express some sceptical, but informed, initial belief. For example, our priors on the slope and intercept:

$$\begin{aligned}\beta_{v,1} &\sim \mathcal{N}(\log(0.45), 1) \\ \beta_{v,2} &\sim \mathcal{N}(0, 20)\end{aligned}$$

Our prior on the location of the intercept ($\beta_{v,1}$) is chance ($\log(0.45)$), and our prior on the location of the slope ($\beta_{v,2}$) is flat (0). In other words, our prior mode is that each condition has no relationship between r and JND and is indistinguishable from chance.

However, this is only the mode: we can use Rensink & Baldridge's data to specify the prior variance of these parameters as encompassing a set of reasonable models by ensuring that believable models are within 1 or 2 standard deviations of the mean of the prior. While Rensink & Baldridge did not fit log-linear models to their data, we can approximate a log fit to the data in their Figure 4 [2], giving an intercept of ~ -1 and slope of ~ -2 . Since $| -1 - \log(.45) | \approx 0.20$, a standard deviation of 1 (variance of 1) will easily cover models having intercepts 2 or 3 times as extreme as the scatterplot condition. If we wish our prior to include all models with an intercept even twice as steep as the scatterplot within 1 standard deviation, a standard deviation of $| -2 \times 2 | = 4$ (variance of 16; conservatively we round up to 20) should suffice.

We use a similar examination of Rensink and Baldridge's Figure 4 to estimate priors on the effect of *approach*, which was around 0.2, meaning a variance of 0.25 easily covers values of approach twice as extreme:

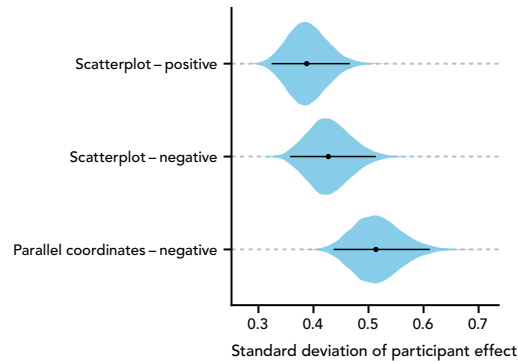


Fig. 5. Posterior distributions of the standard deviation of random effects for participants in the high precision group (τ_v). Higher standard deviation here indicates greater variance in performance between participants. As we do not see evidence that the scatterplot is more variable than its next closest contender for lowest JND (indeed, there is some evidence of the opposite), we can recommend scatterplots as a widely-applicable visualization for correlation.

$$\begin{aligned}\beta_{v,3} &\sim \mathcal{N}(0, 0.25) \\ \beta_{v,4} &\sim \mathcal{N}(0, 0.25)\end{aligned}$$

Finally, we use relatively uninformed priors for variance parameters:

$$\begin{aligned}\sigma_v^2 &\sim \text{InverseGamma}(1, 1) \\ \tau_v^2 &\sim \text{InverseGamma}(1, 1)\end{aligned}$$

We fit the model using MCMC sampling in JAGS [8].⁷

5.3 Performance on a hypothetical set of datasets

We can use our model to derive the expected precision of estimation of a typical individual on an unknown dataset. Rensink & Baldridge [2] proposed doing this (equation 8 in that paper) by integrating the

⁷ Two pilot chains were run, and the Raftery-Lewis diagnostic [12] used to estimate a minimum chain length to convergence of $\sim 70,000$. We then ran two chains with burn-in of 100,000 and sample length of 100,000 each, thinned by 10, for final sample size of 10,000 per chain. Chain starting values (with different random seeds) were set from the

model in Section 4. Convergence was assessed by visual inspection of density plots and autocorrelation plots, and all parameters passed the Gelman-Rubin diagnostic [13] (multivariate potential scale reduction factor < 1.05).

fitted line over a probability distribution of values of r one might expect to encounter in a given domain. Applied to the models in that paper, this method has the disadvantage that cannot derive the uncertainty associated with the calculated average performance, making it impossible to determine differences between visualizations.

However, if we adopt the same approach in a Bayesian framework on models derived from individual observations, uncertainty is straightforward to derive in the form of the posterior distribution of expected JND. We can do this by drawing r values from a hypothetical distribution, for example a uniform distribution over the same space sampled in the experiment (we could use a more specific distribution if we had knowledge of expected correlation values in some domain):

$$r \sim \mathcal{U}(0.3, 0.8)$$

We can then use MCMC sampling⁸ to obtain a posterior distribution of μ_v , the expected JND for the average person given for each visualization \times direction pair:

$$\log(\mu_v) = \beta_{v,1} + \beta_{v,2}r$$

We can then rank visualizations by their expected performance on an unknown dataset (see results, below). Given a problem space with datasets having some known/estimated distribution of r , we can easily re-compute rankings from the model (possibly put in discussion)

6 RESULTS OF FINAL MODEL

Fig. 6.1 shows the results of our model in log space for each visualization. Based on the method outlined above, we roughly group visualization \times direction pairs into a partial ranking based on the expected average person's performance integrated over the fit lines (Fig. 6.2). We can see four groups emerge. We then take the difference between the expected precision between each successive group. This difference (on the log scale) corresponds to a ratio on the original data scale; here we see that the visualizations in each successive group yield at least 1.5x better precision (lower JND) than the previous group on average (Fig. 6.3).

Note how the model accommodates the fact that several of the visualizations have many observations worse than chance. By formulating the model such that we did not have to drop these conditions, we were able to derive estimates of their performance, just with comparatively higher uncertainty — the posterior distributions for those conditions near chance are more diffuse than those with higher precision, and the difference between that group and the low precision group has much more uncertainty associated with it (it should be noted that “indistinguishable from chance” in Fig. 6.2 should be read “indistinguishable from chance so far as this model and data can tell”). Rather than dropping these visualizations as in Harrison *et al.*, we simply *learn less about* them from the model. Given a future experiment designed to be more sensitive to JNDs in this range, we might still use these posteriors as priors in such an analysis.

Finally, it is worth considering the expected variance in performance between individuals. In the best-performing group, we find that variance is fairly similar between conditions (Fig. 5). While parallel coordinates-negative may be slightly more variable, the difference is not credible. However, this is worth investigating further: with more data, we could estimate this difference more precisely, and also judge whether it has practical significance for design implications. For now, all evidence seems to support a general recommendation for the use of scatterplots in all cases — it is in the highest-performing group of visualizations for both negative and positively-correlated data, and its individual variance is comparable to (and likely slightly better than) its nearest contender in average performance (parallel coordinates). It also works equally well for negatively and positively correlated data.

7 DISCUSSION

- Jeff: Discussion should reinforce the main points of the paper throughout: (1) taking individuals into account, choosing appropriate variable transformations, and dealing with outliers, etc (in our case, censoring), and including (and/or culminating in) recommendations for future research, (2) zoom out a bit to talk about perceptual laws and (possibly) the importance of listening to the data over pre-mature theoretical commitments, (3) replication, data-sharing,
- Censoring probably useful in other similar experiments with thresholds that are artifacts of the data collection process.
- Might be something in here about perceptual “laws”, model fitting, individual differences, etc
- Other approaches could have tried --- other transformations, other error distributions, truncation. None fit as well or were as parsimonious as the log transformation.
- Reproducibility, code, data
- An important point of discussion in both Harrison et al. and Rensink and Baldridge is the use of Weber Models for comparison, namely comparing the Weber fraction “k” akin to how one compares the index of performance (1/b) in Fitt's Law models. It seems we should acknowledge and discuss this aspect. Is there a reasonable and similarly simple parameter-based comparison (e.g., beta_v2) afforded by our models? Worth relating to prior work in either case.

8 CONCLUSION

TBD

ACKNOWLEDGMENTS

- Original authors?

REFERENCES

- [1] L. Harrison, F. Yang, S. Franconeri, and R. Chang, “Ranking Visualizations of Correlation Using Weber’s Law,” *IEEE Trans. Vis. Comput. Graph.*, vol. 20, no. 12, pp. 1943–1952, 2014.
- [2] R. A. Rensink and G. Baldridge, “The perception of correlation in scatterplots,” *Comput. Graph. Forum*, vol. 29, no. 3, pp. 1203–1210, 2010.
- [3] T. Hastie, R. Tibshirani, and J. Friedman, *The elements of statistical learning: data mining, inference and prediction*, Second Edi. Springer, 2009.
- [4] T. James, “Estimation of Relationships for Limited Dependent Variables,” *Econometrica*, vol. 26, no. 1, pp. 24–36, 1958.
- [5] T. Amemiya, “Tobit models: A survey,” *J. Econom.*, vol. 24, pp. 3–61, 1984.
- [6] J. K. Kruschke, *Doing Bayesian Data Analysis*. Elsevier Inc., 2011.
- [7] S. H. . Hurlbert, “Pseudoreplication and the Design of Ecological Field Experiments,” *Ecol. Monogr.*, vol. 54, no. 2, pp. 187–211, 1984.
- [8] M. Plummer, “JAGS: A Program for Analysis of Bayesian Graphical Models Using Gibbs Sampling,” *Proc. 3rd Int. Work. Distrib. Stat. Comput. (DSC 2003)*, 2003.
- [9] R. A. Rigby and D. M. Stasinopoulos, “Generalized additive models for location, scale, and shape,” *Appl. Stat.*, vol. 54, no. 3, pp. 507–554, 2005.
- [10] G. E. P. Box and D. R. Cox, “An analysis of transformations,” *J. R. Stat. Soc. Ser. B*, vol. 26, no. 2, pp. 211–252, 1964.
- [11] M. Stone, “An Asymptotic Equivalence of Choice of Model by Cross-Validation and Akaike’s Criterion,” *J. R. Stat. Soc. Ser. B*, vol. 39, no. 1, pp. 44–47, 1977.

⁸ Conducted in the same sampling run used to fit the model.

- [12] A. E. Raftery and S. M. Lewis, "Comment: One Long Run with Diagnostics: Implementation Strategies for Markov Chain Monte Carlo," *Stat. Sci.*, vol. 7, no. 4, pp. 493–497, 1992.
- [13] A. Gelman and D. B. Rubin, "Inference from Iterative Simulation Using Multiple Sequences," *Stat. Sci.*, vol. 7, no. 4, pp. 457–472, 1992.